Available online at www.sciencedirect.com
SCIENCE DIRECT®
International Journal of Heat and Mass Transfer 48 (2005) 1649–1661
International Journal of HEAT and MASS TRANSFER
www.elsevier.com/locate/ijhmt

On heat transfer in gas–solid pipe flows: Effects of collision induced alterations of the flow dynamics

V. Chagras, B. Oesterlé *, P. Boulet

Laboratoire d'Energétique et de Mécanique Théorique et Appliquée, UMR CNRS 7563, ESSTIN, Université Henri Poincaré—Nancy 1, 2 rue Jean Lamour—54519, Vandoeuvre-les-Nancy, France

Received 3 September 2003; received in revised form 9 December 2004

Abstract

An Eulerian–Lagrangian approach is used to model turbulent gas–solid flows in heated pipes. The key problems of dispersion, turbulence modulation and particle collisions are addressed by means of a complete four-way description. In particular, special care has been brought to the effects of both particle–particle and particle–wall collisions, which are known to be important on the dynamical point of view. Dilute or moderately dense suspensions are considered (loading ratio up to 10). Comparison of the numerical results with available experimental data about suspension Nusselt numbers leads to satisfactory agreement in vertical pipe flows and qualitative accordance in the horizontal case. It is confirmed that the collision treatment is a very crucial and sensitive aspect of the global model, in so far that it strongly affects the flow dynamics. The collision induced alteration of the velocity and concentration profiles leads to significant changes in the heat exchange rate. Since the question may arise of possible effect of conductive heat transfer during collisions, this point has been examined too, confirming that the direct thermal exchanges during solid–solid contacts are negligible under the present conditions.

Keywords: Gas–solid flow; Heat transfer; Eulerian–Lagrangian; Particle collisions

1. Introduction

The prediction of gas–solid flows requires several modelling problems to be overcome, among them the description of both flow fields, coupling phenomena, turbulence modulation, and collisional effects. Taking into account two-way coupling and carefully addressing these successive difficulties, numerous studies have contributed to improve the predictions of the dynamics of such flows. However, in spite of a huge application field, including combustion, heat exchanger devices or drying technologies, less attention has been paid to heat transfer in gas–solid flows, which is known to be affected through various mechanisms. First of all, turbulence modulation due to particle–fluid interactions is a key factor, which may be prevailing even at low loadings. The overall heat capacity of the suspension may also be strongly modified, thus inducing heat transfer modulation depending on the loading ratio. Besides such important effects, particle collisions may be expected to play a significant role too since they are able to

* Corresponding author. Tel.: +33 0383 685 080; fax: +33 0383 685 085.
E-mail address: benoit.oesterle@esstin.uhp-nancy.fr (B. Oesterlé).

0017-9310/$ - see front matter © 2005 Elsevier Ltd. All rights reserved.
doi:10.1016/j.ijheatmasstransfer.2004.12.007

Nomenclature

A_c	contact area during collision (m^2)
$C_{M\Omega}$	torque coefficient (/)
c_p	specific heat ($J\ kg^{-1}\ K^1$)
d_p	particle diameter (m)
D	pipe diameter (m)
e	particle–wall restitution coefficient (/)
E	Young modulus (Pa)
f_d	kinetic friction factor (/)
f_s	static friction factor (/)
$\mathbf{F}_D$	drag force (N)
$\mathbf{F}_L$	lift force (N)
$\mathbf{g}$	gravitational acceleration ($m\ s^{-2}$)
h_p	heat transfer coefficient around particles ($W\ m^{-2}\ K^{-1}$)
k	turbulent kinetic energy ($m^2\ s^{-2}$)
L	pipe length (m)
m	solid loading ratio (/)
m_p	particle mass (kg)
N	number density of particles (m^{-3})
Nu	Nusselt number (/)
Pr	Prandtl number (/)
Pr_t	turbulent Prandtl number (/)
q_m	mass flow rate ($kg\ s^{-1}$)
Q_{12}	heat exchange during collision (J)
r	radial co-ordinate (m)
R	pipe radius (m)
Re_p	particle Reynolds number (/)
S_{kf}	turbulent kinetic energy source term ($kg\ m^{-1}\ s^{-3}$)
$S_{\varepsilon f}$	dissipation rate source term ($kg\ m^{-1}\ s^{-4}$)
S_θ	heat transfer source term ($W\ m^{-3}$)
$\mathbf{S}_u$	momentum source term ($N\ m^{-3}$)
$\mathbf{s}_u$	fluctuation of momentum source term ($N\ m^{-3}$)
t_c	contact duration (s)
T_L	fluid Lagrangian time scale (s)
T^*, T^*_θ	integral time scales of the fluid seen (s)
$\mathbf{u}$	fluctuating velocity ($m\ s^{-1}$)
$\mathbf{U}$	instantaneous velocity ($m\ s^{-1}$)
U_c	centerline velocity of the fluid ($m\ s^{-1}$)
V_{12}	impact velocity ($m\ s^{-1}$)
x_i	Cartesian co-ordinates (m)
$\mathbf{X}_p$	particle location (m)
z	axial co-ordinate (m)

Greek symbols

α	solid volume fraction (/)
Δt	time step (s)
ε	dissipation rate of turbulent kinetic energy ($m^2\ s^{-3}$)
Φ	wall flux density ($W\ m^{-2}$)
λ	thermal conductivity ($W\ m^{-1}\ K^{-1}$)
ν	Poisson coefficient (/)
Θ	instantaneous temperature (K)
θ	fluctuating temperature (K)
Θ_m	bulk average temperature (K)
ρ	density ($kg\ m^{-3}$)
σ_γ	standard deviation of virtual wall inclination (/)
τ_c	inter-particle collision time (s)
τ_p	particle relaxation time (s)
Ω_p	particle angular velocity ($rad\ s^{-1}$)
Ω_R	particle relative angular velocity ($rad\ s^{-1}$)
ξ_{fp}	fluid–particle velocity correlation coefficient (/)
ψ_i	random disturbance for velocity ($m\ s^{-1}$)
ψ_θ	random disturbance for temperature (K)

Subscripts and superscripts

f	fluid
p	particle
s	suspension
w	at the wall
i,j,k	in direction x_i, x_j, x_k

strongly affect the dynamics of the two-phase flow even in dilute suspensions with loading ratio below 1 or solid volume fraction α as low as 10^{-4}, as demonstrated by many investigations [1–6]. In particular, the effects of particle–particle collisions and of the nature of particle–wall collisions (effect of wall roughness) upon the dynamical behaviour of the suspension flow have been reported in various situations. It is well recognized that inter-particle collisions reduce the anisotropy of the particle fluctuating motion and enhance the transverse mixing thus flattening the profiles of particle velocity and concentration [4].

It is known [6–8] that the importance of inter-particle collisions is determined by the parameter τ_c/τ_p, where τ_c is the mean inter-particle collision time (or inverse of the collision frequency) and τ_p is the particle relaxation time, the behaviour of the dispersed phase being significantly affected by collisions for $\tau_c/\tau_p < 1$. As the collision frequency is proportional to number density, mean fluctuating velocity and diameter squared of the particles, it is therefore not possible to draw any simple conclusion about the role of inter-particle collisions by only looking at the value of the loading ratio or of the solid volume fraction. According to the estimation provided in Ref. [6,7] for the collision frequency, and examining the data from three available experimental investigations (which will be used later for comparison) about heat transfer in air–solid pipe flows with particle density

$\rho_p \approx 2500$ kg m^{-3}, it can be concluded that inter-particle collisions must be taken into account from the following threshold values of the loading ratio: $m \approx 0.1$ for $d_p = 500$ μm (experiments by Jepson et al. [9]), $m \approx 0.2$ for $d_p = 140$ μm [10], and $m \approx 0.5$ for $d_p = 43$ μm [11].

Various numerical tools devoted to the simulation of non-isothermal gas–solid flows have been developed during the past decade [12–18], The effect of particle collisions upon heat transfer in gas–solid pipe flows was first demonstrated by Louge et al. [12]. Inter-particle collisions were also shown by Mansoori et al. [13] to weaken the temperature fluctuations near the wall and to amplify them in the pipe core region. Recently, an improved Eulerian–Lagrangian simulation has been elaborated and used to study the influence of turbulence modelling on heat transfer [18]. Here, a similar approach is used to investigate the role of both inter-particle and particle–wall collisions upon the wall heat transfer in gas–solid pipe flows. In contrast with the work by Mansoori et al. [13], the effects of wall roughness and particle–wall friction factor are taken into account, as well as particle rotation owing to the high angular velocities induced by frictional particle–wall collisions. Moreover, here inter-particle collisions are handled by means of a probabilistic model. Furthermore, a low-Reynolds approach is used for the simulation of the fluid phase in order to improve the prediction accuracy in the near-wall region.

The paper is organized as follows: the next section is devoted to the description of the continuous phase modelling, the dispersed phase tracking and the collision treatment; the key features of the numerical method and processing are addressed in Section 3; finally, numerical results obtained in vertical and horizontal turbulent gas–solid flows are presented and discussed in Section 4, where emphasis is put on the effect of considering inter-particle collisions, and on the influence of the particle–wall collision parameters. At rather high loading ratio, the question may arise of the possible effect of conductive heat transfer during collisions, therefore this point is also examined. In order to cover a wide range of particle size, comparisons are provided with the three above-mentioned experiments [9–11].

2. Model description

Before describing the complete formulation, the major assumptions and numerical choices are to be recalled. A turbulent air–solid flow in a heated pipe is considered, with rigid, spherical and mono-dispersed particles. The temperature variations are small enough for radiative transfer and fluid property alterations due to temperature to be negligible. The two-phase flow is simulated using an Eulerian scheme for the continuous phase and Lagrangian tracking for the dispersed phase. A four-way coupling scheme is applied in the present model. Air–particle interactions are taken into account by means of appropriate source terms in the gas phase equations and iterative numerical processing. Inter-particle collisions are handled through special procedures during the trajectory computation as described farther on.

2.1. Continuous phase

The present model has received complete validation in one-phase flow situation through comparisons with Nagano's data-base [19]. This validation step is required for the part of the simulation dedicated to the gas phase, even if it does not imply that the obtained accuracy still holds for two-phase flows. The authors are aware that the model constants or functions were optimized for single phase flows and might require some adjustments to take into account the presence of the dispersed phase, however such model refinements are not available in the literature at present time, unfortunately. Yet, it may be mentioned that validation tests were also achieved in two-phase flow situation through comparison with the measurements by Tsuji et al. [20] in a gas–solid pipe flow. Satisfactory agreement regarding the velocity profiles and turbulence modulation was obtained, as extensively discussed in Boulet and Moissette [18], where a detailed presentation of the formulation can be found.

Standard phase-averaged equations for mass, momentum and energy conservation are complemented by a NEVM approach (non-linear eddy viscosity model) for turbulent stresses and by the WET closure (from "wealth ≈ earnings × time" [21]) for turbulent heat fluxes. This last point is the only difference in the continuous phase formulation as compared to Ref. [18], in which a GGDH model (generalized gradient diffusion hypothesis) was used. In the present work, turbulent heat fluxes are therefore computed as in [21], namely:

$$\langle u_{fj}\theta_f\rangle = -C_t f_{\mu t}\frac{k_f}{\varepsilon_f}\left(\langle u_{fj}u_{fk}\rangle\frac{\partial\langle\Theta_f\rangle}{\partial x_k} + \langle u_{fk}\theta_f\rangle\frac{\partial\langle U_{fj}\rangle}{\partial x_k}\right) \quad (1)$$

where brackets indicate phase-averaged quantities. The difference between the GGDH and WET models lies in the term involving the velocity gradients which is not addressed in the GGDH model. As this contribution cannot be a priori assumed to be negligible, especially in the near-wall region, it was decided to implement it in our model. Such a combination of the NEVM and WET closure relationships for the Reynolds stresses and turbulent heat fluxes was tested and recommended by Rokni and Sunden [22] in a paper devoted to the simulation of heat transfer in duct flows. The WET model was proven to accurately predict the temperature profiles and turbulent heat fluxes, and to yield very good comparison

with available Nusselt number correlations in straight ducts [22].

As demonstrated in [18], the proposed formulation combines the simplicity and robustness of the k–ε approaches, as compared to a Reynolds Stress Model for example, with the advantage of taking turbulence anisotropy into account. Finally, it must be mentioned that low-Reynolds effects are considered according to the model of Myong and Kasagi [23], in order to avoid the problem of using standard wall functions to deal with the near-wall layer. Therefore a very fine grid is required near the wall, given that the width of the first mesh should be about 0.6 wall units. Special care must therefore be brought in the computation of the source terms due to particles, as described later in Section 2.2.2.

Owing to the problem geometry (the suspension is flowing in a circular pipe), the governing equations have been written in cylindrical co-ordinates for numerical handling. In vertical configurations the fluid characteristics are predicted with radial and axial variations only. The solution is slightly more involved in horizontal configurations, where the flow is not axisymmetric due to the influence of gravity which makes the dispersed phase concentration higher in the bottom part of the duct. The resulting angular variation of the source terms requires handling the problem in a fully three-dimensional way.

2.2. Dispersed phase

Each Lagrangian step consists in the computation of a large number of particle trajectories (typically 10^5), with the fluctuating quantities of the fluid seen by the particles being calculated according to the dispersion model described below (Section 2.2.1), using the data provided by the Eulerian calculation of the gaseous phase flow field. In the first Lagrangian step, inter-particle collisions are not considered. From the second Lagrangian step, such collisions are included as described in Section 2.2.3. After each Lagrangian step, a new Eulerian computation of the gas flow field is performed, this iterative process being repeated until convergence. Particles are tracked individually by solving the following balance equations in order to calculate their instantaneous position, velocity, rotational velocity and temperature:

$$\frac{\mathrm{d}\mathbf{X}_\mathrm{p}}{\mathrm{d}t} = \mathbf{U}_\mathrm{p} \tag{2}$$

$$m_\mathrm{p}\frac{\mathrm{d}\mathbf{U}_\mathrm{p}}{\mathrm{d}t} = \mathbf{F}_\mathrm{D} + \mathbf{F}_\mathrm{L} + m_\mathrm{p}\mathbf{g} \tag{3}$$

$$m_\mathrm{p}\frac{d_\mathrm{p}^2}{10}\frac{\mathrm{d}\Omega_\mathrm{p}}{\mathrm{d}t} = -\frac{\pi}{64}C_{\mathrm{M}\Omega}\rho_\mathrm{f}d_\mathrm{p}^5\|\Omega_\mathrm{R}\|\Omega_\mathrm{R} \tag{4}$$

$$m_\mathrm{p}c_{pp}\frac{\mathrm{d}\Theta_\mathrm{p}}{\mathrm{d}t} = h_\mathrm{p}\pi d_\mathrm{p}^2(\Theta_\mathrm{f} - \Theta_\mathrm{p}) \tag{5}$$

Eq. (3) involves the drag force $\mathbf{F}_\mathrm{D}$, which is computed following the Morsi and Alexander's correlation for the drag coefficient [24], and the Magnus lift force $\mathbf{F}_\mathrm{L}$ due to the Magnus effect, which has to be taken into account owing to the high rotational velocities induced by particle–wall and particle–particle collisions, and is computed following the proposal by Oesterlé and Bui Dinh [25]. The shear lift force has been omitted mainly due to lack of information about the way to take it into account in the present situation. Available data usually address the case of linear shear flows and very small particle Reynolds numbers [26–28], which is far from the present case where massive particles may be involved and where realistic pipe flow is considered. Moreover, from the correlation proposed by Mei [29] for intermediate Reynolds numbers, the effect of shear lift force can be shown to be less important than the Magnus effect in case of significant angular velocities of particles. The torque coefficient $C_{\mathrm{M}\Omega}$ appearing in Eq. (4) is expressed by means of the correlation proposed by Dennis et al. [30]. The heat transfer coefficient h_p is computed using the following standard correlation for the particle Nusselt number:

$$Nu_\mathrm{p} = \frac{h_\mathrm{p}d_\mathrm{p}}{\lambda_\mathrm{f}} = 2 + 0.6Re_\mathrm{p}^{0.6}Pr^{0.33} \tag{6}$$

where Re_p is the instantaneous particle Reynolds number and Pr is the Prandtl number of the gas. All these fluid–particle interactions (force, torque, heat exchange) involve the instantaneous velocity of the fluid at the particle location, which is predicted by means of an anisotropic dispersion model as described hereafter.

2.2.1. Dispersion model

In order to reproduce the effect of the fluid turbulence upon the particle motion and temperature, the instantaneous properties of the fluid phase have to be simulated in accordance with the averaged values provided by the Eulerian model for the continuous phase. This is achieved using a stochastic method as suggested and validated in Moissette et al. [31], where the fluid fluctuating velocities and temperature at time t and particle location $\mathbf{X}_\mathrm{p}(t)$ are generated by means of first order stochastic processes consistent with Langevin-type equations. With the purpose of making this dispersion model applicable for anisotropic and non-homogeneous turbulence, improvements have been brought to the stochastic process as described in [32], in order to obtain the prescribed values of the fluid Reynolds stresses (known from the Eulerian calculation) and to take their variation into account to avoid any spurious drift of fluid particles towards the low turbulence intensity regions [33,34]. The final form of the stochastic process used to predict the fluid fluctuating velocity is (see [32] for details):

$$u_{\mathrm{f}i_n} = u_{\mathrm{f}i_{n-1}} \exp\left(-\Delta t/T_i^*\right) + T_i^*\left(1-\exp\left(-\Delta t/T_i^*\right)\right)\left(\frac{\partial\langle u_{\mathrm{f}i}u_{\mathrm{f}j}\rangle}{\partial x_j}\right) + \psi_{i_n} \quad (7)$$

where $u_{\mathrm{f}i_n}$ is the ith component of the velocity fluctuation of the at time $t = n\Delta t$ and position $X_{\mathbf{p}}(t)$, T_i^* stands for the integral time scale of the fluid seen by the particle and the ψ_{i_n} are Gaussian random variables with zero mean value and covariance matrix obtained from stationarity requirements under quasi-homogeneity conditions:

$$\langle\psi_{i_n}\psi_{j_n}\rangle = \left[1-\exp\left(-\Delta t\left(\frac{1}{T_i^*}+\frac{1}{T_j^*}\right)\right)\right]\langle u_{\mathrm{f}i}u_{\mathrm{f}j}\rangle \quad (8)$$

A simple procedure to generate such random numbers ψ_{i_n} is to select ψ_{1_n} from a Gaussian probability density function with zero mean and variance obeying $\langle\psi_{1_n}^2\rangle = \left(1-\exp\left(-2\Delta t/T_1^*\right)\right)\langle u_{\mathrm{f}1}^2\rangle$, and to build ψ_{2_n} and ψ_{3_n} by $\psi_{2_n} = a_0\varphi + a_1\psi_{1_n}$ and $\psi_{3_n} = b_0\chi + b_1\psi_{1_n} + b_2\psi_{2_n}$, where φ,χ are independent Gaussian variables with zero mean and variance unity, and the coefficients a_k, b_k are deduced from Eq. (8).

The integral Lagrangian time scales T_i^* of the fluid seen by the particles are computed according to the expressions proposed in [32], which the reader is referred to for further details. These expressions account for flow anisotropy, inertia effect and crossing trajectory effect.

The temperature fluctuations are generated according to a similar method as for the velocity, i.e. the temperature increment of the fluid seen by a discrete particle is assumed to obey a Langevin equation, which results in the following stochastic process:

$$\theta_{\mathrm{f}_n} = \theta_{\mathrm{f}_{n-1}} \exp\left(-\frac{\Delta t}{T_\theta^*}\right) + \left(1-\exp\left(-\frac{\Delta t}{T_\theta^*}\right)\right)\left(\frac{\partial\langle u_{\mathrm{f}i}\theta_{\mathrm{f}}\rangle}{\partial x_j}\right) + \psi\theta_n \quad (9)$$

where the second term in the r.h.s. accounts for the inhomogeneity of the turbulence, and the variance of the Gaussian perturbation ψ_θ is prescribed from stationarity requirement of the process:

$$\langle\psi_{\theta_n}^2\rangle = \left[1-\exp\left(-2\Delta t/T_\theta^*\right)\right]\langle\theta_{\mathrm{f}}^2\rangle \quad (10)$$

Moreover, in order to ensure consistency of the generated temperature fluctuations with the required values of the fluid velocity–temperature correlations $\langle u_{\mathrm{f}r}\theta_{\mathrm{f}}\rangle$and $\langle u_{\mathrm{f}z}\theta_{\mathrm{f}}\rangle$, ψ_θ has to be connected with the corresponding random terms in the velocity fluctuation generation process, in such a manner that:

$$\langle\psi_{\theta_n}\psi_{j_n}\rangle = \left[1-\exp\left(-\Delta t\left(\frac{1}{T_\theta^*}+\frac{1}{T_j^*}\right)\right)\right]\langle u_{\mathrm{f}j}u_{\mathrm{f}}\rangle \quad (11)$$

Such conditions can easily be fulfilled by selecting a random number ζ from a Gaussian distribution with mean zero and variance unity, and building ψ_{θ_n} by $\psi_{\theta_n} = a_\theta\zeta + b_\theta\psi_{r_n} + c_\theta\psi_{z_n}$, where the coefficients a_θ, b_θ and c_θ are obtained from the conditions on $\langle\psi_{\theta_n}^2\rangle$ and $\langle\psi_{\theta_n}\psi_{j_n}\rangle$. The temperature integral time scale of the fluid seen by the particles, T_θ^*, is estimated assuming that the ratio of temperature to velocity time scales is approximately equal to the ratio of the corresponding diffusivities, which leads to $T_\theta^*/T_z^* \approx Pr_{\mathrm{t}}^{-1}$, where Pr_{t} is the turbulent Prandtl number. The fluid turbulent heat fluxes are provided by the Eulerian model for the fluid phase and the variance of the fluid temperature is evaluated from the following approximate relationship (derived from the second-order moment equation for $\langle\theta_{\mathrm{f}}^2\rangle$ in neglecting the diffusion term):

$$\langle\theta_{\mathrm{f}}^2\rangle \cong -\frac{2}{C_{\varepsilon\theta}}\frac{k_{\mathrm{f}}}{\varepsilon_{\mathrm{f}}}\langle u_{\mathrm{f}r}\theta_{\mathrm{f}}\rangle\frac{\partial\langle\Theta_{\mathrm{f}}\rangle}{\partial r} \quad (12)$$

where $C_{\varepsilon\theta}$ was fixed to 2 after comparison with the data base of Nagano et al. [19].

2.2.2. Source term formulation

Source terms have to be introduced into the governing equations to allow the influence of the dispersed phase on the continuous phase to be taken into account. These terms are computed at the end of each Lagrangian step, following the relationships presented in Table 1. Whereas the momentum and heat transfer source terms are standard ones (drag force, lift force and heat exchange by convection around particles are taken into account as sources for the continuous phase), the formulation of particle–turbulence interactions is less common, however. For large particles, the source term for turbulent kinetic energy, $S_{k\mathrm{f}}$, is expressed following the analysis by Crowe [35], which has been recently discussed and used by Lain et al. [5] and Boulet and Moissette [18]. In these studies, a new form for $S_{k\mathrm{f}}$ has been combined with a standard balance for the source term for dissipation, the constant $C_{\varepsilon 3}$ being fixed to 1.8 in [18] according to a sensitivity analysis in a case close to the present one, whereas Lain et al. [5] suggested a value of 1 in the case of a horizontal channel.

The following analysis may help to understand the difficulty which arises in the modelling of $S_{k\mathrm{f}}$ and of

Table 1
Expressions used for the source terms

Source term	Eulerian–Lagrangian formulation
$\langle S_{u_i}\rangle$	$N\left\langle -m_{\mathrm{p}}\left(\frac{\mathrm{d}U_{\mathrm{p}i}}{\mathrm{d}t}-g_i\right)\right\rangle$
$\langle S_\theta\rangle$	$N\left\langle h_{\mathrm{p}}\pi d_{\mathrm{p}}^2(\Theta_{\mathrm{p}}-\Theta_{\mathrm{f}})\right\rangle$
$S_{k\mathrm{f}}$ (standard formulation for small particles)	$\langle s_{u_i}u_{\mathrm{f}i}\rangle$
$S_{k\mathrm{f}}$ (tentative formulation for large particles)	$\left\lvert\langle S_{u_i}\rangle\langle U_{\mathrm{f}i}-U_{\mathrm{p}i}\rangle\right\rvert + \langle s_{u_i}u_{\mathrm{p}i}\rangle$
$S_{\varepsilon\mathrm{f}}$	$C_{\varepsilon 3}\frac{\varepsilon_{\mathrm{f}}}{k_{\mathrm{f}}}S_{k\mathrm{f}}$ with $C_{\varepsilon 3}=1.8$

the source term for the dissipation rate equation, $S_{\varepsilon f}$. When using a k–ε model, it is assumed that particles are smaller than the smallest turbulent eddies. Some turbulent production may take place close to the particles, due to the no-slip condition at particle surface and to wake formation, an effect called "pseudo-turbulence". The term corresponding to this contribution may be obtained, when deriving the turbulent kinetic energy balance, as a part of the exchanges at the interface between the two phases. As the expected length scale of the corresponding eddies is of the order of the particle diameter, the contribution of the pseudo-turbulence may lie in contradiction with the former hypothesis of "particles being smaller than the turbulent eddies". A complementary difficulty is that the ratio k_f/ε_f is commonly introduced as a characteristic time scale for the largest turbulent eddies and used in the dispersion models during the Lagrangian tracking. When using the full source term expression, one introduces eddies at different scales (the largest ones but also others as small as the particles) in the turbulent kinetic energy balance. Thus, the question of the exact significance of the scale k_f/ε_f arises. Furthermore, the extra-production or pseudo-turbulence has to be associated with a corresponding extra-dissipation. A common strong assumption is therefore to consider that the extra-dissipation exactly compensates the extra-production. In agreeing with this hypothesis one avoids a theoretical difficulty, since the part of the eddies which are smaller than the particles are no more included in the calculation of the turbulent kinetic energy. There is a drawback with this common solution, however, since the remaining part of the source term (without the extra-production) is known to be always negative. This may lead to wrong predictions since large particles have been observed to generate turbulence, as is well known. A solution has to be found to provide a way to simulate this turbulence increase.

In order to obtain such a turbulence increase for large particles, we decided to use the formulation by Crowe [35] which includes the extra-production term in the source term for the turbulent kinetic energy, without any supplementary hypothesis concerning the associated extra-dissipation. It is only included in $S_{\varepsilon f}$, the constant $C_{\varepsilon 3}$ being adapted to yield correct turbulence modulation in two-phase flow configurations. Actually, this choice consists in using a formulation which has been observed to provide acceptable numerical results [18], although it is not completely satisfactory on the theoretical point of view. On the contrary, usual forms of the source terms which can only result in turbulence decrease have produced abnormal data or even numerical divergence (due to zero or negative values for k_f). When small particles are considered however, our experience is that the above-discussed formulation is no more able to yield satisfactory prediction of the turbulence modulation (numerical divergence often occurs), therefore the standard formulation of the source terms has been used in our computations in this case.

Additionally, let us mention that due the strong grid tightening associated with the use of a low-Reynolds number model, the particle diameter may exceed the mesh width in the near wall region. In this case, the source terms are distributed over several cells according to the particle surface area pertaining to each cell.

2.2.3. Collision treatment

For each particle, the above-explained trajectory computation is reinitialized after any collision with the wall or with another particle. Simulation of such collisions requires some empirical parameters such as the static and kinetic friction factors and the coefficient of restitution e, which are needed to express the particle translational and rotational velocities after the collision using the impulsive equations and Coulomb's law [2]. For particle–wall collisions, the "virtual wall" model of Sommerfeld [36] is used in order to account for the effect of wall roughness and particle shape (departure from sphericity). In this model, the actual wall is replaced by a virtual wall, whose inclination angle obeys a Gaussian distribution with given standard deviation σ_γ and zero mean value. The so-called shadow effect is included in the model. Some examples are given in Section 4 to illustrate the effect of the collision parameters upon the flow dynamics and heat transfer.

In order to avoid handling the particle–particle interactions in a deterministic way, which requires to simultaneously compute the trajectories of all the particles present in the flow domain (a method limited by present computer capacities due to the huge number of particles in actual flows), interparticle collisions are taken into account following the probabilistic method suggested by Oesterlé and Petitjean [2]. In this method, the occurrence of a collision is decided, at each time step, according to a collision probability depending on the local concentration and properties of the two-phase flow. The collision probability is obtained from the expression of the interparticle collision frequency corrected to account for the correlated motion of neighbouring particles [37]:

$$\frac{1}{\tau_c} = \pi N d_p^2 \sqrt{\frac{16}{\pi}\frac{2}{3}k_p}\sqrt{1-\xi_{fp}^2} \tag{13}$$

where N is the number of particles per unit volume, k_p is the fluctuating kinetic energy of the particles and ξ_{fp} stands for the fluid–particle velocity correlation, defined by:

$$\xi_{fp} = \frac{k_{fp}}{\sqrt{k_f k_p}} \tag{14}$$

with $2k_{fp} = \langle u_{fi} u_{pi} \rangle$ being the covariance of the fluctuating velocities of the two phases. The occurrence of a collision during the time interval Δt can be decided by generating a random number with uniform distribution

between 0 and 1, and comparing it with the probability of collision which is $1 - \exp(-\Delta t/\tau_c)$ [2]. If a collision occurs, the tracked particle is supposed to hit a fictitious particle whose velocity is generated in taking into account the correlation of the velocities seen by both particles, as suggested by Sommerfeld [3], according to:

$$u_{\mathrm{fict},i} = R(\tau_p/T_L)u_{p,i} + \sigma_i \xi \sqrt{1 - R(\tau_p/T_L)^2} \quad (15)$$

where $u_{\mathrm{fict},i}$ is the fluctuation of the ith velocity component of the fictitious particle and $u_{p,i}$ is the corresponding value of the tracked particle. Here σ_i is the local rms value of the ith particle velocity component and ξ is a Gaussian random number with zero mean and variance unity. $R(\tau_p/T_L)$ is a correlation function given by the following empirical expression [3]:

$$R(\tau_p/T_L) = \exp(-0.55(\tau_p/T_L)^{0.4}) \quad (16)$$

The position of the impact point is chosen according to a uniform probability on the disc corresponding to the effective collision cross-section. Through the described procedure, the velocity components after collision can be computed [2], and the trajectory calculation process can be restarted.

If heat transfer due to conduction during a collision has to be considered, the jump in particle temperature can be computed using the analytical expression suggested by Sun and Chen [38] for the heat exchanged between two impacting particles:

$$Q_{12} = \frac{0.87 C_{12}(\Theta_2 - \Theta_1) A_c \sqrt{t_c}}{(\rho_{p1} c_{p1} \lambda_{p1})^{-1/2} + (\rho_{p2} c_{p2} \lambda_{p2})^{-1/2}} \quad (17)$$

where Θ_1, Θ_2 are the temperatures of the two particles, c_{p1}, c_{p2} are their specific heats, ρ_{p1}, ρ_{p2} their mass densities and λ_{p1}, λ_{p2} their thermal conductivities. The coefficient C_{12}, which may take values between 1 and 5, can be computed as a function of the Fourier number $\alpha_{p1} t_c / A_c$ (α_{p1} being the thermal diffusivity of particle 1), the ratio $\lambda_{p1}/\lambda_{p2}$ and the ratio $\rho_{p1} c_{p1}/\rho_{p2} c_{p2}$ [38]. The contact area and the contact time are given by $A_c = \pi(5 m_{12} V_{12}^2 d_{12}^2 / 16 E_{12})^{2/5}$ and $t_c = 2.94(5 m_{12}/4 E_{12})^{2/5}(2/V_{12}\, d_{12})^{1/5}$ where V_{12} is the impact velocity and m_{12}, d_{12}, E_{12} are defined by: $m_{12} = \left(m_{p1}^{-1} + m_{p2}^{-1}\right)^{-1}$, $d_{12} = \left(d_{p1}^{-1} + d_{p2}^{-1}\right)^{-1}$, $E_{12} = (4/3)\left((1 - v_1^2)E_1^{-1} + (1 - v_2^2)\, E_2^{-1}\right)^{-1}$ with m_{pi}, d_{pi}, E_i and v_i denoting the masses, diameters, Young moduli and Poisson coefficients of the two particles. In case of particle–wall collisions, the same formulae can be applied considering that d_{p2} and m_{p2} tend to infinity.

3. Numerical processing

All the details concerning the numerical processing may be found in Boulet and Moissette [18]. An iterative scheme is applied in order to allow four-way coupling to be taken into account. In the first iteration, the pure gas flow is computed, then successive loops are performed involving a Lagrangian tracking step followed by the Eulerian computation of the continuous phase flow. Source terms are computed statistically after each Lagrangian step, as discussed above in Section 2.2.2, and are introduced into the gas balance equations after under-relaxation, in order to enhance the stability of the whole numerical code in case where coupling between the two phases becomes too strong. In spite of special carefulness however, it must be said that at present some difficulties still arise during the numerical computation in the horizontal pipe configuration, especially for high values of the roughness parameter. The corresponding instability could be due to the very small mesh width in the near wall area,which makes the dynamics alteration due to particles very difficult to address, a problem supposed to be more critical in rough pipes due to complex rebounds. This assumption has to be confirmed and the corresponding problem is currently being investigated in order to improve the prediction capabilities of the numerical code. On the contrary, no such problem occurs in the vertical pipe configuration, probably due to the axisymmetry which prevents us from too strong discrepancies in the local particle concentration.

Some of typically used numerical parameters are as follows:

- about 50,000 particles are injected in vertical pipe configurations and 100,000 in the horizontal pipe case (tests carried out with 500,000 particles did not indicate any significant influence on the statistical computations); such a large number of particle trajectories is needed in order to get enough particles in each cell for the reliability of statistics and satisfactory assessment of the source terms.
- 40 loops between Eulerian and Lagrangian steps are generally required to achieve convergence for the two-phase flow dynamics, 30 supplementary loops are added to deal with the thermal part of the problem.
- the grid is tightened near the heated section entrance and near the wall in a logarithmic manner with, for the horizontal case for example: 40 nodes in the radial direction, 40 in the axial one and 24 angular locations.

4. Results

Three experiments about non-isothermal gas–particle pipe flows have been extensively studied. In each of them, the flow is dynamically fully developed before

entering the heated section where a constant wall heat flux is prescribed in cases hereafter referred as 1 and 3, whereas a wall temperature is fixed in case 2.

The first one (case 1), taken from the experimental study by Jepson et al. [9], involves relatively massive particles: sand particles with mean diameter 500 μm and loading ratio ranging from 0 to more than 10, so that collisions can be expected to play a significant role. Additional conditions are: pipe diameter $D = 0.0381$ m, length of heated section $L = 3.65$ m, Reynolds numbers 31,000 and 46,500, inlet temperature 293 K, constant wall heat flux $\Phi = 1000$ W m^{-2}.

Case 2 is taken from Farbar and Depew [10] and involves intermediate size particles, namely glass beads of diameter 140 μm. The experimental data used for comparison with our numerical computations are: upwards vertical flow, $D = 0.0175$ m, $L = 1$ m, loading ratio from 0 to 4, Reynolds number around 26,500, inlet temperature 293 K, fixed wall temperature 352 K. In this particular case where various physical phenomena may be expected to be significant, a specific study is presented about the effects of the collision parameters.

The last case investigated here (case 3) is taken from a more recent experimental study by Aihara et al. [11], where small glass particles (diameter 43 μm) are injected in a horizontal pipe. In this situation, the dispersion model may have a strong influence and particle trajectories could be less governed by collisions. Additional effects may take place due to non-symmetrical distributions, since gravity makes the particles move preferentially in the bottom of the pipe. The resulting stratification could therefore enhance the particle–particle collisions at least in this particular area. Other conditions are: $D = 0.0545$ m, $L = 7.6$ m, Reynolds number 120,000, inlet temperature 280 K, constant wall heat flux $\Phi = 896$ W m^2.

Unless otherwise stated, the collision parameters are set to $e = 0.9$ (restitution coefficient) and $f_s = f_d = 0.2$ (static and kinetic friction factors). The value of the roughness parameter σ_γ is varied in terms of the particle diameter according to Lain et al. [5]. In each case, the validity of the complete model when compared with experimental data is first discussed. Then the effect of collisions is further examined, in particular by observing the results obtained for the concentration, velocity and temperature distributions when some parts of the collision model are omitted. Whereas particle–wall collisions are always taken into account for the prediction of the flow dynamics, computations have been carried out and compared with or without particle–particle collisions, with or without taking into account heat transfer due to conduction during collisions, and finally in varying some collision parameters.

In cases 1 and 3 (constant wall heat flux), the suspension Nusselt number is computed according to the following definition:

$$Nu_s = \frac{\Phi D}{(\Theta_w - \Theta_m)\lambda_f} \tag{18}$$

where Θ_m is the suspension bulk temperature:

$$\Theta_m = \Theta_{m_{inlet}} + \frac{\pi D L \Phi}{q_{mf} c_{pf} + q_{mp} c_{pp}}, \tag{19}$$

with $\Theta_{m_{inlet}}$ denoting the temperature at the entrance of the heated section of the pipe. In case 3 (horizontal pipe), the wall temperature Θ_w varies with angular position, thus resulting in azimuthal variations of Nu_s.

In case 2, where the wall temperature is fixed, the Nusselt number is expressed in terms of the logarithmic mean temperature difference ΔT_{Ln} based on inlet and outlet bulk temperatures, as suggested by Farbar and Depew [10]:

$$Nu_s = \frac{\Phi D}{\lambda_f \Delta T_{Ln}} \tag{20}$$

with the wall heat flux Φ computed from $\pi D L \Phi = (q_{mf} c_{pf} + q_{mp} c_{pp})(\Theta_{m_{outlet}} - \Theta_{m_{inlet}})$. Note that only the asymptotic values of the Nusselt number obtained at the pipe outlet are presented hereafter.

4.1. Case 1. Vertical pipe loaded with massive particles

In this case, the experiments by Jepson [9] show that Nu_s first decreases at low loading ratio, and then increases as more particles are injected. As can be seen in Fig. 1, where the computed and measured Nusselt numbers (normalized by the value in pure gas flow, Nu_0) are plotted as a function of the loading ratio m, this trend is well reproduced by the simulation and satisfactory agreement is obtained between the experimental data and the predictions. Nevertheless, it must be emphasized that any extrapolation of the numerical results beyond $m = 10$ would be hazardous, particularly in the case of Fig. 1b where the increase in Nu_s at $m > 5$ is obviously underestimated since following the predicted trend would lead us to conclude that $Nu_s < Nu_0$ even at m of order of 20, which is incorrect. The reason for this underestimation of Nu_s at higher loading probably lies in some inaccurate prediction of the turbulence modulation for such large particles, due to the difficulty in properly modelling the dissipation source term $S_{\varepsilon f}$ as discussed in Section 2.2.2.

Focusing on the effect of particle–particle interactions at intermediate loading ratio of about 1–5, the most important observation is that the difference in suspension Nusselt numbers predicted with or without inter-particle collisions may reach about 8%. Although it cannot be concluded from Fig. 1 that taking inter-particle collisions into account leads to better agreement, the heat transfer rate would be underestimated if particle–particle interactions were omitted. Moreover, it may be noticed that the effect of conductive heat exchange during collisions is negligible (see Fig. 1(b)) because

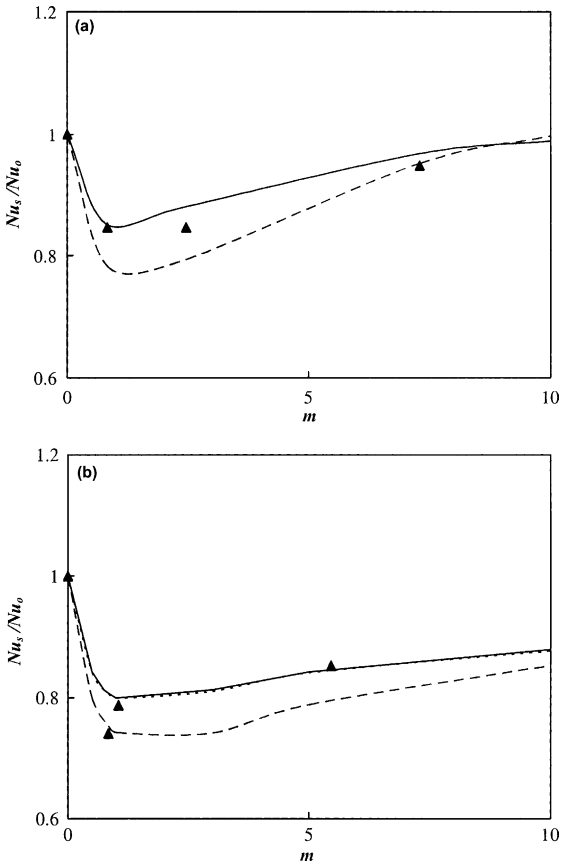

Fig. 1. Normalized Nusselt number in the conditions of case 1 as a function of the loading ratio for various collision modelling conditions ($\sigma_\gamma = 0.06$). Experimental data by Jepson et al. [9]: (▲). Numerical predictions: dashed line, without particle–particle collisions; solid line, with collisions and without heat transfer during contacts; dotted line, with collisions and with heat transfer during contacts ((b) only). Pipe Reynolds number 31 000 (a) and 46 500 (b).

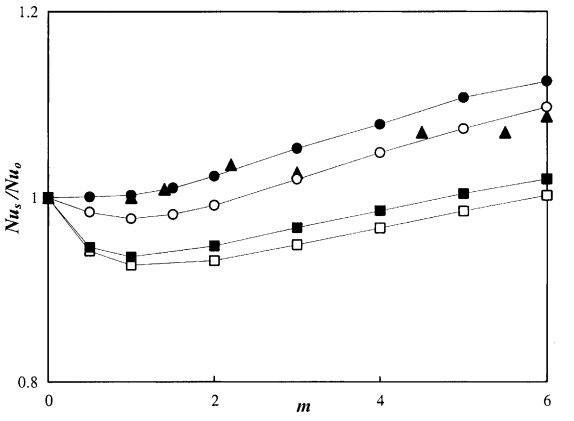

Fig. 2. Normalized Nusselt number in a vertical pipe as a function of the loading ratio, in the conditions of Farbar and Depew [10] (case 2). Experimental data: (▲). Numerical predictions: (□, ■), $\sigma_\gamma = 0.04$; (○, ●), $\sigma_\gamma = 0.1$ (open symbols: without particle–particle collisions, black symbols: with collisions).

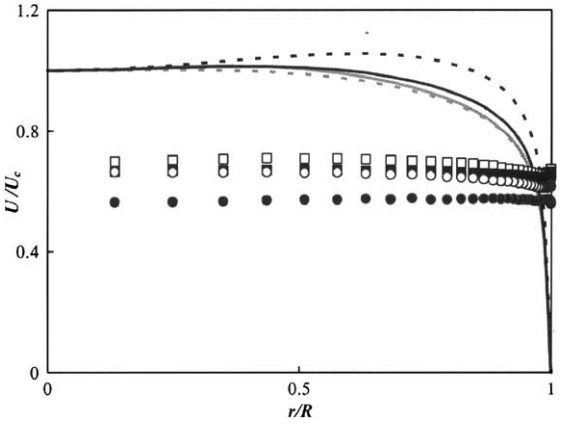

Fig. 3. Velocity profiles in the conditions of case 2, $m = 4$, for two values of σ_γ. Particles: same caption as Fig. 2. Gas: gray lines $\sigma_\gamma = 0.04$, black lines $\sigma_\gamma = 0.1$, solid lines: without collisions, dashed lines: with collisions.

the contact duration and contact area are too small to allow appreciable heat conduction between particles, even at loading ratio of the order of 10. Consequently, in the following sections comparisons are presented for the predictions with and without the effects of particle–particle collisions upon the flow dynamics taken into account, since addressing or not the conductive heat transfer during contacts would give exactly the same results. Let us recall here that "with or without collisions" only refers to particle–particle collisions, since particle–wall collisions are of course always taken into account.

4.2. Case 2. Vertical pipe flow loaded with medium size particles

The results obtained for case 2 are illustrated in Figs. 2–7. In Fig. 2, where the asymptotic Nusselt number Nu_s is presented as a function of the loading ratio, a comparison is provided between our numerical predictions and the experimental data by Farbar and Depew [10] for 140 μm particles. As in the previous case, Nu_s is initially decreasing, passing through a minimum at $m \approx 1$, and then increases with increasing loading ratio. Satisfactory accuracy may be obtained in the numerical prediction provided particle–particle collisions are addressed and the particle–wall collision parameters are carefully chosen. As such parameters may have a strong influence, two values of the roughness parameter σ_γ were tested here, namely 0.04 and 0.1. Fig. 2 shows that, according to the value of σ_γ, the numerical results are in weak or

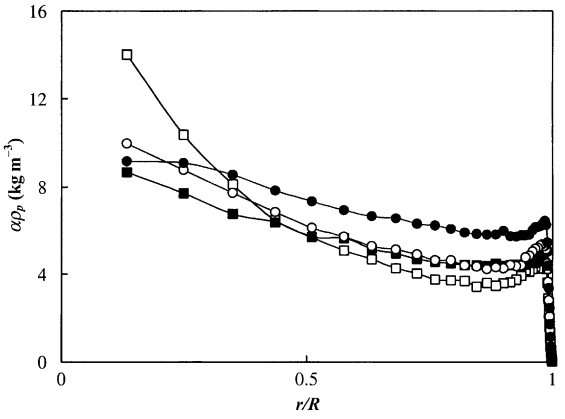

Fig. 4. Particle concentration profiles in the conditions of case 2, $m = 4$, for two values of σ_γ. Same caption as Fig. 2.

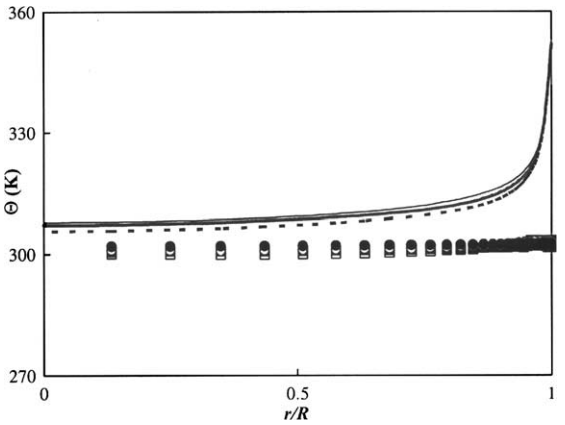

Fig. 5. Temperature profiles in the conditions of case 2, $m = 4$, for two values of σ_γ. Same caption as Fig. 3.

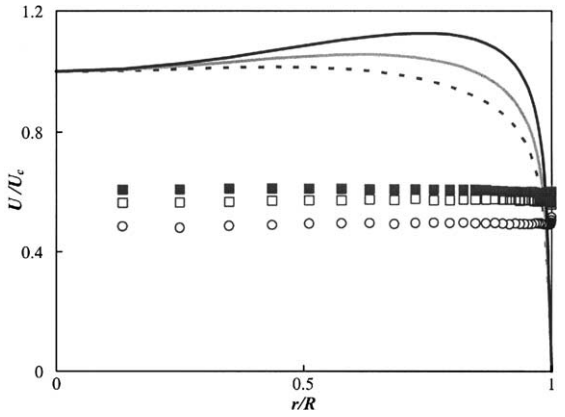

Fig. 6. Velocity profiles in the conditions of case 2, $m = 4$, $\sigma_\gamma = 0.1$. Gas: black solid line, $e = 0.9$, $f_d = 0.4$; gray solid line, $e = 0.9$, $f_d = 0.2$; dashed line, $e = 0.7$, $f_d = 0.2$. Particles: (○), $e = 0.9$, $f_d = 0.4$; (□), $e = 0.9$, $f_d = 0.2$; (■), $e = 0.7$, $f_d = 0.2$.

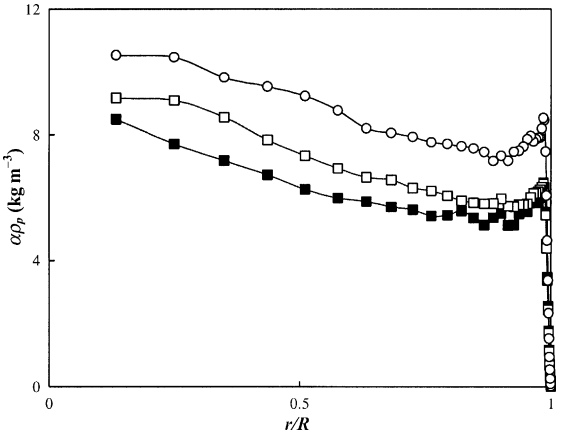

Fig. 7. Particle concentration profiles in the conditions of case 2, $m = 4$, $\sigma_\gamma = 0.1$. (○): $e = 0.9$, $f_d = 0.4$; (□): $e = 0.9$, $f_d = 0.2$; (■): $e = 0.7$, $f_d = 0.2$.

correct agreement with the experimental data, an observation which raises the question of the exact value for this parameter, if achievable. Anyway, it can be concluded that the role of particle–particle collisions on heat exchange is obvious, as well as the characteristics of the particle–wall collisions.

The profiles of velocity, concentration and temperature are presented in Figs. 3–5 in conditions analogous to the previous case, at $m = 4$. Whatever the value of σ_γ, the presence of inter-particle collisions is seen to flatten the particulate phase profiles due to enhanced mixing, and to reduce the solid phase velocity (Fig. 3). This effect is even more pronounced if σ_γ grows, as a consequence of a similar enhancement of the transverse particle motion with increasing wall roughness. The decrease in particle velocity is accompanied by a subsequent increase in mass concentration in the main part of the pipe section. Near the pipe axis, inter-particle collisions are seen to reduce the level of maximum concentration (Fig. 4). In the present case of intermediate particle size and loading, the gas velocity profile may exhibit a maximum shifted from the pipe center towards the wall, as can be seen in Fig. 3 for the higher value of σ_γ (also visible in Fig. 6 below). Clearly, the effects of inter-particle collisions and particle–wall roughness parameter are less marked for the temperature profiles, as shown by Fig. 5. From these observations, inter-particle collisions may be finally expected to affect the heat transfer rate, at least in an indirect manner, due to the alteration of the flow dynamics.

The influence of the particle–wall collision parameters may be further analyzed in examining the influence of the restitution and friction coefficients upon the velocity and concentration profiles. This is the focus of Figs. 6 and 7 where such distributions are presented for various sets of the collision parameters. The velocity and con-

centration profiles are significantly affected by both the dynamic friction coefficient f_d and the restitution coefficient e. The influence of the static friction coefficient is found to be negligible (not shown here). The distributions keep the same pattern as the collision parameters are modified, but it can be seen that the particle velocity increases and the concentration decreases with decreasing f_d or e. As a consequence, even if the temperature distributions are hardly affected by the particle–wall collision parameters in the present case (not shown here), a small reduction of the Nusselt number was nevertheless obtained with decreasing f_d or e.

4.3. Case 3. Horizontal pipe loaded with small glass particles

In this part we deal with a slightly different application where dispersion phenomena could also affect the results and where non-symmetrical patterns are expected due to gravity effects. Actually, this kind of flow loaded with smaller particles is not easy to simulate without encountering some divergence problems when taking into account two-way or four-way coupling effects. Mainly due to the fact that the turbulence modulation source terms lead to exaggerated decrease in turbulent kinetic energy for such small particles, simulations may become difficult to perform in satisfactorily stable conditions. Nevertheless, four-way coupling has though to be addressed, since discrepancies are observed on the gas phase when compared to the pure gas case. This is the reason why the results presented here are for moderate loading ratio. In Fig. 8, an example is given of numerical predictions of Nu_s in terms of the loading ratio obtained in conditions close to the experiments presented by Aihara et al. [11], with distinction between the top and the bottom of the pipe. Comparisons between the numerical and experimental data show that our predictions, even if not quantitatively correct, are in qualitative agreement with the experiments regarding the difference between the upper and lower walls. The Nusselt number is found to be smaller at the bottom wall than at the top, an effect probably due to higher particle concentration in the lower region of the pipe which tends to reduce the air velocity as compared to the top region of the pipe. Heat transfer is seen to be affected by particle–particle collisions, but it is difficult to really observe any improvement when taking the collisions into account, due to the qualitative nature of the comparison. What is certain however is that heat transfer by contact during collisions has no effect on the results, as previously mentioned.

As explained above, it is interesting to notice that in the present horizontal configuration the proposed model is able to reproduce the non-symmetrical pattern of the Nusselt number distribution, as shown by Fig. 9 where the azimuthal distribution of the asymptotic suspension

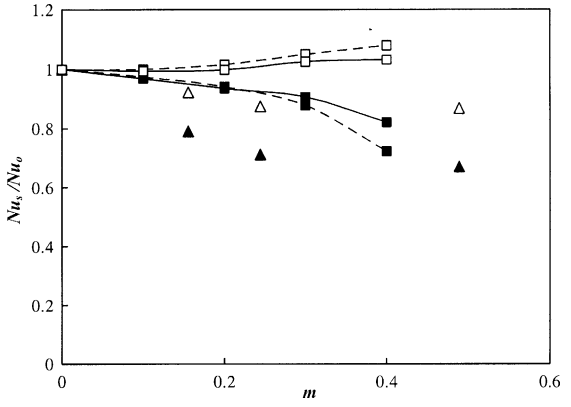

Fig. 8. Normalized Nusselt number in a horizontal pipe as a function of the loading ratio for various collision modelling conditions (conditions of case 3, $\sigma_\gamma = 0.01$). Open symbols: top; black symbols: bottom. Experimental data by Aihara et al. [11]: (△, ▲). Numerical predictions: (□, ▲) (dotted line: without particle–particle collisions; solid line: with collisions).

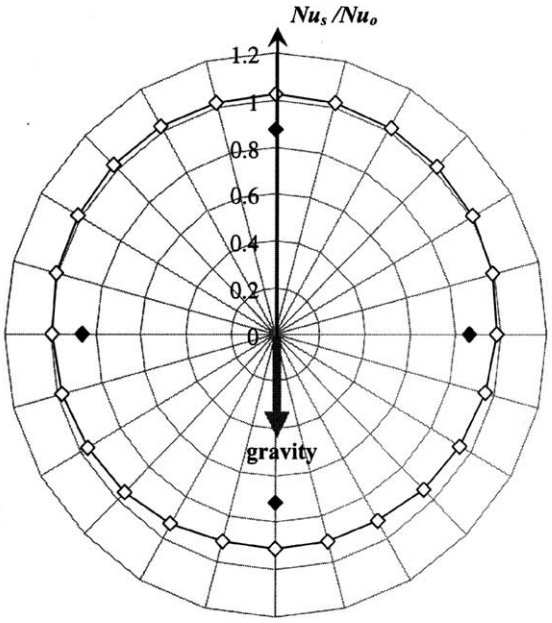

Fig. 9. Azimuthal distribution of the normalized Nusselt number in the conditions of case 3, $m = 0.3$, $\sigma_\gamma = 0.01$. Black symbols: experiments [11].

Nusselt number Nu_s is displayed at loading ratio $m = 0.3$. In this plot, the ratio Nu_s/Nu_0 is plotted as a function of the angular coordinate and compared to the experimental measurements by Aihara et al. [11] in the same conditions. Even if the decrease in Nusselt number is not accurately predicted by the numerical simulation, the ability of the simulation code to capture such an asymmetry, at least qualitatively, is well

demonstrated here, especially in what concerns the comparison between the top and bottom values of Nu_s. Finally, it may be mentioned that the effects of the particle–wall collision parameters were also investigated, leading to opposite conclusions as compared to the previous case regarding the influence of the restitution coefficient and the roughness parameter. Actually, in this case Nu_s was found to slightly decrease with increasing σ_y and increasing e, contrary to the behaviour observed in case 2 and illustrated by Fig. 2 as regards σ_γ. There is as yet no satisfactory explanation for such opposite observations, considering the complexity of the involved phenomena and the major differences between cases 2 and 3, i.e. particle size, pipe orientation, thermal boundary conditions.

5. Conclusions

The role of collisions undergone by particles has been investigated in a non-isothermal gas–solid pipe flow. The main conclusion is that the flow dynamics alterations induced by particle–particle collisions and by the features of particle–wall collisions result in significant modulation of the heat exchanges. In particular, the particle–particle collisions have been found to increase the overall heat transfer by as much as 8% in vertical pipe flow. On the contrary, it has been confirmed that direct heat transfer modification due to possible conductive exchanges during collisions is negligible in the range of loading ratio investigated here (up to 10).

It has been shown that satisfactory predictions of a suspension pipe flow in non-isothermal conditions may be obtained, provided the key problem of collision treatment is carefully addressed. Despite some remaining difficulties especially associated to particle–turbulence interactions, good agreement with available experimental data has been achieved in vertical pipes. Although the horizontal configuration is more difficult to address, qualitative agreement has been obtained in this case.

The sensitivity of the predictions to the physical parameters involved in the particle–wall collision modelling has been emphasized, showing that such data would require further investigations in order to avoid too strong uncertainties. Among such parameters, the most influential one is undoubtedly σ_γ which characterizes the dispersive nature of collisions due to wall roughness.

References

[1] M. Sommerfeld, G. Zivkovic, Recent advances in the numerical simulation of pneumatic conveying through pipe systems, in: Ch. Hirsch (Ed.), Computational Methods in Applied Sciences, Proceedings of the 1st European Computational Fluid Dynamics Conference and the 1st European Conference on Numerical Methods in Engineering, Brussels, Belgium, 1992, pp. 201–212.

[2] B. Oesterlé, A. Petitjean, Simulation of particle-to-particle interactions in gas–solid flows, Int. J. Multiphase Flow 19 (1993) 199–211.

[3] M. Sommerfeld, Inter-particle collisions in turbulent flows: a stochastic Lagrangian model, in: Proceedings of the 1st International Symposium on Turbulence and Shear Flow Phenomena, Santa Barbara, CA, USA, 1999, pp. 265–270.

[4] Y. Yamamoto, M. Potthoff, T. Tanaka, T. Kajishima, Y. Tsuji, Large-eddy simulation of turbulent gas-particle flow in a vertical channel: effect of considering inter-particle collisions, J. Fluid Mech. 442 (2001) 303–334.

[5] S. Lain, M. Sommerfeld, J. Kussin, Experimental studies and modelling of four-way coupling in particle-laden horizontal channel flow, Int. J. Heat Fluid Flow 23 (2002) 647–656.

[6] M. Sommerfeld, Validation of a stochastic Lagrangian modelling approach for inter-particle collisions in homogeneous isotropic turbulence, Int. J. Multiphase Flow 27 (2001) 1829–1858.

[7] C.T. Crowe, M. Sommerfeld, Y. Tsuji, Multiphase Flows with Droplets and Particles, CRC Press, Boca Raton, 1998.

[8] A. Kartushinsky, E.E. Michaelides, An analytical approach for the closure equations of gas–solid flows with inter-particle collisions, Int. J. Multiphase Flow 30 (2004) 159–180.

[9] G. Jepson, A. Poll, W. Smith, Heat transfer from gas to wall in a gas–solids transport line, Trans. Inst. Chem. Eng. 41 (1963) 207–211.

[10] L. Farbar, C.A. Depew, Heat transfer effects to gas–solid mixtures using solid spherical particles of uniform size, Indust. Eng. Chem. Fundament. 2 (1963) 130–135.

[11] T. Aihara, K. Yamamoto, K. Narusawa, T. Haraguchi, M. Ukaku, A. Lasek, F. Feuillebois, Experimental study on heat transfer of thermally developing and developed, turbulent, horizontal pipe flow of dilute air–solids suspensions, Heat Mass Transfer 33 (1997) 109–120.

[12] M. Louge, J.M. Yusof, J.T. Jenkins, Heat transfer in the pneumatic transport of massive particles, Int. J. Heat Mass Transfer 36 (1993) 265–275.

[13] Z. Mansoori, M. Saffar-Avval, H. Basirat-Tabrizi, G. Ahmadi, S. Lain, Thermo-mechanical modeling of turbulent heat transfer in gas–solid flows including particle collisions, Int. J. Heat Fluid Flow 23 (2002) 792–806.

[14] K.S. Han, H.J. Sung, M.K. Chung, Analysis of heat transfer in pipe carrying two-phase gas–particle suspension, Int. J. Heat Mass Transfer 34 (1991) 69–78.

[15] R. Avila, J. Cervantes, Analysis of the heat transfer coefficient in a turbulent particle pipe flow, Int. J. Heat Mass Transfer 38 (1995) 1923–1932.

[16] P. Boulet, S. Moissette, R. Andreux, B. Oesterlé, Test of an Eulerian–Lagrangian simulation of wall heat transfer in a gas–solid pipe flow, Int. J. Heat Fluid Flow 21 (2000) 381–387.

[17] P. Boulet, V. Chagras, S. Moissette, Double velocity correlation and turbulent heat flux predictions in gas–solid flows, in: W. Rodi, N. Fueyo (Eds.), Proceedings of the 5th International Symposium on Engineering Turbulence Modelling and Measurements, Mallorca, Spain, 2002, pp. 929–938.

[18] P. Boulet, S. Moissette, Influence of the particle–turbulence modulation modelling in the simulation of a non-isothermal gas–solid flow, Int. J. Heat Mass Transfer 45 (2002) 4201–4216.
[19] Y. Nagano, N. Kasagi, H. Kawamura, M. Maeda, H. Maekawa, T. Takagi, Transport processes of heat and momentum in the wall region of turbulent pipe flow, in: Data-base on Turbulent Heat Transfer, Available from: http://www.jsme.or.jp/ted/HTDB/dathet.html, Nagoya Institute of Technology, Japan, 1990.
[20] Y. Tsuji, Y. Morikawa, H. Shiomi, LDV measurements of an air–solid two-phase flow in a vertical pipe, J. Fluid Mech. 139 (1984) 417–434.
[21] B. Launder, An introduction to single-point closure methodology, in: T.B. Gatski, M.Y. Hussaini, J.L. Lumley (Eds.), Simulation and Modeling of Turbulent Flows, Oxford University Press, 1996, pp. 243–310.
[22] M. Rokni, B. Sunden, Improved modeling of turbulent forced convective heat transfer in straight ducts, J. Heat Transfer 121 (1999) 712–719.
[23] H.K. Myong, N. Kasagi, A new approach to the improvement of k–ε turbulence model for wall-bounded shear flows, JSME Int. J. Series II 33 (1990) 63–72.
[24] S.A. Morsi, A.J. Alexander, An investigation of particle trajectories in two-phase flow systems, J. Fluid Mech. 55 (1972) 193–208.
[25] B. Oesterlé, T. Bui Dinh, Experiments on the lift of a spinning sphere in a range of intermediate Reynolds numbers, Exp. Fluids 25 (1998) 16–22.
[26] P. Saffman, The lift on a small sphere in a slow shear flow, J. Fluid Mech. 22 (1965) 385–400, and Corrigendum 31 (1968) 624.
[27] J. McLaughlin, Inertial migration of a small sphere in linear shear flows, J. Fluid Mech. 224 (1991) 261–274.
[28] Q. Wang, K. Squires, M. Chen, J. McLaughlin, On the role of the lift force in turbulence simulations of particle deposition, Int. J. Multiphase Flow 23 (1997) 749–763.
[29] R. Mei, An approximate expression for the shear lift force on a spherical particle at finite Reynolds number, Int. J. Multiphase Flow 18 (1992) 145–147.
[30] S.C.R. Dennis, S.N. Singh, D.B. Ingham, The steady flow due to a rotating sphere at low and moderate Reynolds numbers, J. Fluid Mech. 101 (1980) 257–279.
[31] S. Moissette, B. Oesterlé, P. Boulet, On the influence of dispersion modelling in Eulerian–Lagrangian predictions, in: Proceedings of the 4th International Conference on Multiphase Flow, New Orleans, LA, USA, 2001, Paper no. 393.
[32] M. Khalij, A. Tanière, B. Oesterlé, Combined effects of particle–wall interactions and turbulent dispersion in gas–solid flows using accurate Lagrangian stochastic modelling, in: H.A. Mang, F.G. Rammerstorfer, J. Eberhardsteiner (Eds.), Proceedings of the 5th World Congress on Computational Mechanics (WCCM V), Vienna, Austria, 2002, Paper no. 80092.
[33] B.J. Legg, M.R. Raupach, Markov chain simulation of particle dispersion in inhomogeneous flows: the mean drift velocity induced by a gradient in Eulerian velocity variance, Bound. Layer Meteorol. 24 (1982) 3–13.
[34] J.M. Mclnnes, F.V. Bracco, Stochastic particle dispersion modeling and the tracer-particle limit, Phys. Fluids A 4 (1992) 2809–2824.
[35] C.T. Crowe, On models for turbulence modulation in fluid–particle flows, Int. J. Multiphase Flow 26 (2000) 719–727.
[36] M. Sommerfeld, Modelling of particle–wall collisions in confined gas–particle flows, Int. J. Multiphase Flow 18 (1992) 905–926.
[37] J. Laviéville, O. Simonin, A. Berlemont, Z. Chang, Validation of inter-particle collision models based on Large Eddy Simulation in gas–solid turbulent homogeneous shear flow, in: Proceedings of the ASME Fluids Engineering Division Summer Meeting, Vancouver, Canada, 1997, Paper no. 3623.
[38] J. Sun, M.M. Chen, A theoretical analysis of heat transfer due to particle impact, Int. J. Heat Mass Transfer 31 (1998) 969–975.